Numerical study of the impact of inoculant and grain transport on macrosegregation and microstructure formation during solidification of an Al-22%Cu alloy

Knut Omdal Tveito, Marie Bedel, Miha Založnik, Hervé Combeau, Mohammed M'Hamdi, Arvind Kumar, Pradip Dutta

▶ **To cite this version:**

Knut Omdal Tveito, Marie Bedel, Miha Založnik, Hervé Combeau, Mohammed M'Hamdi, et al.. Numerical study of the impact of inoculant and grain transport on macrosegregation and microstructure formation during solidification of an Al-22%Cu alloy. IOP Conference Series: Materials Science and Engineering, 2012, 33, 10.1088/1757-899X/33/1/012089 . hal-01710319

HAL Id: hal-01710319
https://hal.univ-lorraine.fr/hal-01710319

Submitted on 15 Feb 2018

HAL is a multi-disciplinary open access archive for the deposit and dissemination of scientific research documents, whether they are published or not. The documents may come from teaching and research institutions in France or abroad, or from public or private research centers.

L'archive ouverte pluridisciplinaire **HAL**, est destinée au dépôt et à la diffusion de documents scientifiques de niveau recherche, publiés ou non, émanant des établissements d'enseignement et de recherche français ou étrangers, des laboratoires publics ou privés.

Distributed under a Creative Commons Attribution 4.0 International License

Numerical study of the impact of inoculant and grain transport on macrosegregation and microstructure formation during solidification of an Al-22%Cu alloy

To cite this article: K O Tveito *et al* 2012 *IOP Conf. Ser.: Mater. Sci. Eng.* **33** 012089

View the article online for updates and enhancements.

Related content

- Influence of transport mechanisms on nucleation and grain structure formation in DC cast aluminium alloy ingots
M Bedel, M Založnik, A Kumar et al.
- Three-dimensional study of macro- and mesosegregation formation in a rectangular cavity cooled from one vertical side
V F De Felice, K O Tveito, M Založnik et al.
- The effect of finite microscopic liquid solute diffusion on macrosegregation formation
K O Tveito, M Bedel, M Založnik et al.

This content was downloaded from IP address 193.48.49.224 on 15/02/2018 at 17:00

Numerical study of the impact of inoculant and grain transport on macrosegregation and microstructure formation during solidification of an Al-22%Cu alloy

K O Tveito[1], M Bedel[2], M Založnik[2], H Combeau[2], M M'Hamdi[1,3], A Kumar[2] and P Dutta[4]

[1] Dept. of Materials Technology, NTNU, N-7491 Trondheim, Norway
[2] Institut Jean Lamour, Département SI2M, CNRS – Université de Lorraine,Ecole des Mines de Nancy, Parc de Saurupt CS14234, F-54042 Nancy cedex, France
[3] SINTEF Materials and Chemistry, N-0314 Oslo, Norway
[4] Department of Mechanical Engineering, Indian Institute of Science, Bangalore, India

E-mail: knut.tveito@material.ntnu.no

Abstract. We investigate the impact of the nucleation law for nucleation on Al-Ti-B inoculant particles, of the motion of inoculant particles and of the motion of grains on the predicted macrosegregation and microstructure in a grain-refined Al-22 wt.% Cu alloy casting. We conduct the study by numerical simulations of a casting experiment in a side-cooled 76x76x254 mm sand mould. Macrosegregation and microstructure formation are studied with a volume-averaged two-phase model accounting for macroscopic heat and solute transport, melt convection, and transport of inoculant particles and equiaxed grains. On the microscopic scale it accounts for nucleation on inoculant particles with a given size distribution (and corresponding activation undercooling distribution)and for the growth of globular solid grains. The growth kinetics is described by accounting for limited solute diffusion in both liquid and solid phases and for convective effects. We show that the consideration of a size distribution of the inoculants has a strong impact on the microstructure(final grain size) prediction. The transport of inoculants significantly increases the microstructure heterogeneities and the grain motion refines the microstructure and reduces the microstructure heterogeneities.

1. Introduction

The prediction of the microstructure formation during solidification is of major importance for the industry. Micro-macro models are developed for decades now to relate the macroscopic solidification conditions to the microscopic structures obtained. Rappaz [1] gives an overview of the microscopic mechanisms of microstructure formation and the coupling between them and the macroscopic transport phenomena.

A crucial point of the microscopic modelling is nucleation. As recalled in[2], the nucleation is rarely homogeneous as it is energetically more favourable for the metal to solidify on foreign particles which are always, deliberately or not, present in the metal. Heterogeneous nucleation is not easy to calculate, as even a known distribution of refiner particles, deliberately added into the liquid metal, can be modified by the fragmentation of grains or by the agglomeration of particles. However, different nucleation models were developed, which are used in the macroscopic models.

Published under licence by IOP Publishing Ltd

When the experimental average grain density is known, an easy way to avoid modelling the inoculants activation is to consider an initial grain density in the melt entering the mould which matches the experimental data[3]. The grains are not generated but only redistributed by the flow. But when inoculants are taken into account, their modelling is most of the time very simplified. All the inoculants are usually supposed to be activated instantaneously at the liquidus or at a given undercooling, as justified in[4]. More rarely, an inoculant size distribution is considered trough a normal law and is discretized in classes [5]. Though there is no reason to justify that the inoculants remain fixed when the liquid moves, inoculants transport was never considered until now. Thus the goal of this study is to analyse the impact of the inoculant motion on the macrosegregation and the microstructure formation. An experiment is modelled with different hypotheses in order to see the impact of each phenomenon.

2. Model description

The model is an extension of the volume-averaged two-phase model and the solution algorithm that was described in detail in [6].Only the extensions as well as the main features of the model are presented here. The model describes and couples phenomena at two scales, which are considered to be distinct. At the macroscopic scale the transport of momentum, mass, heat, solute, grain, and inoculants are described by volume-averaged transport equations. At the microscopic scale the nucleation and the growth of globular grains are described by volume-averaged interfacial balances. The liquid flow and the movement of globular grains are described on a macroscopic level by considering the buoyancy-driven flow arising from the liquid density variations (thermo-solutal convection),the density differences between liquid and solid, and the drag forces at the grain interfaces. The Boussinesq approximation is used, and in the present work the shrinkage-induced flow is neglected. When the volume fraction of solid exceeds the imposed packing fraction, the solid phase is assumed to be stationary and the liquid interfacial drag is described with a Darcy term modelled by the Kozeny-Carman law. On a microscopic level, the model takes into account finite diffusion of solute in liquid and solid phases and assumes local thermal equilibrium and thermodynamic equilibrium at the solid-liquid interface.

Nucleation of grains is assumed to occur on grain-refiner (inoculant) particles. According to the athermal nucleation theory of Greer and co-workers [5],the critical undercooling for free growth of a grain on an inoculant particle of diameter d is given by $\Delta T_c(d)=4\Gamma/d$ where Γ is the Gibbs-Thomson constant. The number of activated particles then depends on the size distribution of the particle population, which can be represented by an exponential distribution density function: $n(d)=N_0/d_0.\exp(-d/d_0)$ [m^{-4}], where N_0 [m^{-3}]is a characteristic inoculant population density and d_0[m] is the characteristic width of the distribution. This representation holds for particles large enough. In the modelling, the size distribution is discretized into m classes of inoculants. Each class is represented by a population density N^i_{nuc} and a critical undercooling $\Delta T_c{}^i=4\Gamma/d^i$, depending on the average inoculant diameter of the class d^i. When the local solutal undercooling reaches the critical undercooling of the class, its inoculant density, N^i_{nuc}, is added to the grain density, N_G, and N^i_{nuc} becomes locally zero. The conservation equations for the density of each inoculant class and the grain density are Equations (1) and (2), respectively, where Φ^i represents the transfer from inoculants to grains upon nucleation. The inoculants are assumed to be transported by the liquid with its velocity and one conservation equation is solved separately for each class.

$$\frac{\partial\left(N^i_{nuc}\right)}{\partial t}+\nabla\cdot\left(N^i_{nuc}\left\langle\vec{v}_l\right\rangle^l\right)=-\Phi^i \quad , \quad \Phi^i=\begin{cases}N^i_{nuc}\delta(t) & , \Delta T>\Delta T^i_c \\ 0 & , \text{else}\end{cases} \quad , \quad i=1,...,m \tag{1}$$

$$\frac{\partial\left(N_G\right)}{\partial t}+\nabla\cdot\left(N_G\left\langle\vec{v}_s\right\rangle^s\right)=\sum_{i=1}^{m}\Phi^i \tag{2}$$

3. Experiment description and its modelling

The two-phase model is applied to the experiment of Kumar et al.[7], concerning horizontal solidification of a grain-refined (0.05 wt.% TiB_2) Al-22wt.%Cu alloy. The details of the experiment can be found in Ref. [7]. Here, an illustration of the experimental setup is provided in Figure 1a, showing the graphite chill and the cast cavity including its dimensions.

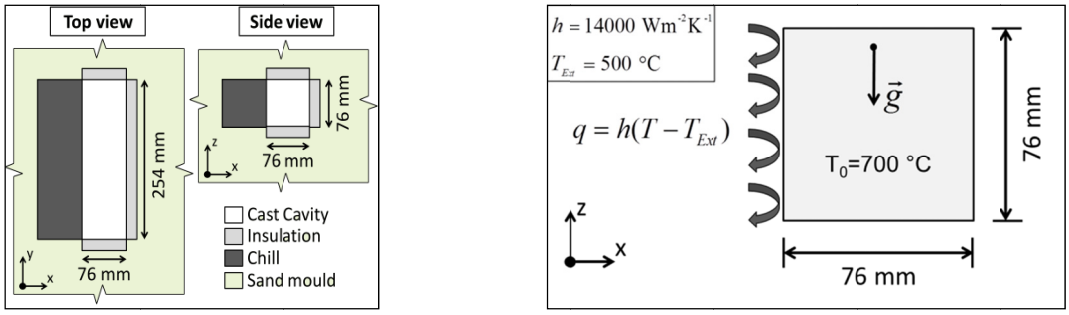

(a) (b)

Figure 1. (a) Illustration of experiment geometry and (b) 2D model for numerical simulations.

The experiment is modelled as a2D problem in the *xz* plane as shown in Figure 1b. The cooling heat flux along the left boundary is modelled with a Fourier condition, while the other boundaries are assumed to be thermally insulated. N conditions are assigned to all boundaries and the initial temperature is 700 °C. The thermophysical data are given in Table. The constant solute diffusion coefficients in the liquid and solid phases were calculated from [8] at 599 °C, the liquidus temperature of the nominal alloy. The liquidus slope and melting point were adjusted to better fit the phase diagram for high concentrations of copper. The liquid and solid densities are constant and equal, except for the buoyancy term in the momentum equations, where the liquid density is taken from [7]. The liquid, the solid and the average ($\rho_{average}=g_l\rho_l+g_s\rho_s$) densities are shown as function of solid fraction in Figure 2, by using the lever rule model for the solidification path. We can notice that even when the grains move, the buoyancy effect increases with the solid fraction as it depends on the average density. The packing fraction is set to 0.27[7] and a columnar zone with stationary solid phase is assumed for the first 10 mm from the chill.

Table 1. Modified thermophysical data Al-22wt.%Cu alloy

Property	Unit	Value
Diffusion coefficient, solid	$m^2\ s^{-1}$	4.2×10^{-13}
Diffusion coefficient, liquid	$m^2\ s^{-1}$	3.8×10^{-9}
Thermal conductivity, solid	$W.m^{-1}.°C^{-1}$	120.7
Thermal conductivity, liquid	$W.m^{-1}.°C^{-1}$	57.3
Specific heat (liquid and solid)	$J.kg^{-1}.°C^{-1}$	1100
Characteristic length used in Kozeny Carman law	m	50×10^{-6}
Pseudo Al melting temperature	°C	703.86
Liquidus slope	°C wt.%$^{-1}$	-4.766
Eutectic temperature	°C	548
Partition coefficient	-	0.173
Reference liquid density	$kg\ m^{-3}$	2800.00
Solid density (buoyancy)	$kg\ m^{-3}$	2609.45
Thermal coefficient of volumetric expansion (β_T)	°C^{-1}	1.17×10^{-4}
Solutal coefficient of volumetric expansion (β_s)	(wt.%)$^{-1}$	-7.3×10^{-3}
Dynamic viscosity, liquid	$N.s.m^{-2}$	1.2×10^{-3}
Packing fraction (gs)	-	0.27
Gibbs-Thomson coefficient	K.m	1.9×10^{-7}

The size distribution for grain refiner particles is taken from [9], for 5kg/t of inoculants of type TiB_2(instead of the 0.5kg/t used in the experiment, in order to limit the undercooling). The distribution is modelled by an exponential function with the parameters $N_0=3.56 \times 10^{12}\ m^{-3}$ and $d_0=7.1 \times 10^{-7}$ m, for inoculant diameters between 1 and 10 μm. The distribution, when usually represented as a function of the particle diameter, is continuously decreasing. However, when expressed as a function of the critical undercooling, this distribution reaches a maximum at around 0.5°C, as can be seen in Figure 3. In the present study, the distribution is discretized into 15 classes: undercooling intervals are defined by increasing step from 0.1 to 0.95°C. The inoculant density distribution and the undercooling

intervals used for the discretization are shown in Figure 3. Note that the exponential law was extrapolated to particles smaller than 0.1 µm to cover the whole range of undercoolings.

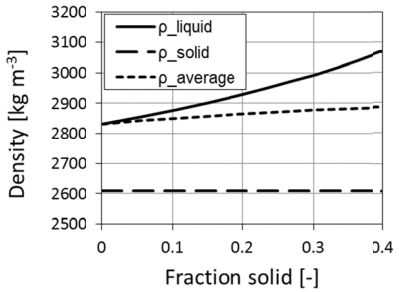

Figure 2. Densities versus the solid fraction, lever rule model.

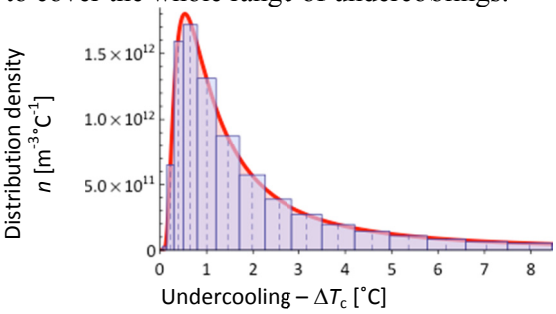

Figure 3. Distribution density function of the inoculant population (red line) and inoculant classes (blue bars). The surface of a bar corresponds to the inoculant population volume density N^i_{nuc}[m^{-3}] of a class and $\Delta T_c{}^i$ are indicated as dashed lines.

The transport equations are solved with a Finite Volume Method and the SIMPLE-method for staggered grid is used for pressure-velocity coupling. The convective terms are discretized with a first-order upwind scheme and for time discretization a fully implicit first-order scheme is used. For all simulations an equidistant grid of 40x40 cells and constant time step of 10^{-3}s is used.

4. Numerical results

In order to study the impact of the different phenomena on the macrosegregation formation and the microstructure, the four cases are defined with an increasing complexity. Their main characteristics are defined in Table 2. The first case is used as a reference for the macrosegregation formation: only natural convection is taken into account at the macro-scale, and all the inoculant classes are instantaneously activated at the liquidus. The inoculant density is taken as the sum of the 15 inoculant class densities defined in the previous section. Then for the Case2, the inoculant distribution is taken into account so that the local grain density depends on the reached undercooling. In Case3, the inoculants can move with the liquid and the local grain density additionally depends on inoculant transport. Finally, in Case 4, the grain motion is taken into account. In all the cases, the inoculants are uniformly distributed in the melt at t=0s.

Table 2. Cases definition

	Case 1	Case 2	Case 3	Case 4
Nucleation at the liquidus	x			
Nucleation function of the undercooling		x	x	x
Inoculant motion			x	x
Grain motion				x

4.1. Case 1: Reference case

The inoculantsandthe grains are assumed to be fixed, and the grain density is homogeneous throughout the cavity. All the inoculant classes (which correspond to an initial inoculant density of 3.135x10^{12} m^{-3}) are activated locally as soon as the local temperature reaches the liquidus.

The final macrosegregation pattern for Case 1 is shown in Figure 8a. The cooling from the left hand boundary introduces a horizontal temperature gradient and thermo-solutal convection results in a counter-clockwise flow pattern. Within the mushy zone the rate of segregation is described by the conservation equation for the average composition C_m:

$$\frac{\partial C_m}{\partial t} = -g_l \left\langle \vec{v}_l \right\rangle^l \cdot \nabla \left\langle C_l \right\rangle^l = -\frac{1}{m} g_l \left\langle \vec{v}_l \right\rangle^l \cdot \nabla \left[T - \Delta T_s \right] \quad , \quad T = T_m + m C_l^* \quad , \quad \Delta T_s = m\left(C_l^* - \left\langle C_l \right\rangle^l \right) \qquad \textbf{(3)}$$

where g_l is the volume fraction liquid, $\langle v_l \rangle^l$ is the intrinsic liquid velocity, m is the liquidus slope, C_l^* is the interface composition and $\langle C_l \rangle^l$ is the average liquid composition. The influence of the gradients of undercooling is dependent on the liquid Fourier number ($Fo_l = D_l t_{solidification}/R_f^2$, where R_f is the final grain radius). In the entire cavity, the liquid Fourier number is higher than 100, and according to Ref. [10], the influence of the gradients of undercooling on macrosegregation formation is then small. Within the mushy zone, negative segregation is formed in the upper part of the cavity where the liquid flows in the opposite direction of the temperature gradient, while a severe positive segregation is formed in the lower part of the cavity where the liquid flows in the same direction than the temperature gradient. This segregation pattern can be easily understood from Equation (3).

4.2. Case 2: Impact of inoculant distribution (neither inoculant nor grain motion)

By accounting for the inoculant size distribution, the competition between nucleation and growth is included in the model. As the inoculants and the grains are fixed for Case 2, the number of activated inoculant classes, and thus the final grain density, only depends on the maximum local undercooling. Generally, the solidification kinetics results in higher undercoolings reached at higher cooling rates.

The local cooling rate, and thus the undercooling, attains the highest values close to the cooled left-hand boundary where up to 12 inoculant classes are activated, resulting in a higher grain density. With increasing distance from the cooled boundary the local cooling rate and undercooling decreases, and the grain density decreases accordingly as shown in the horizontal profile in Figure 4a for Case 2.

In the present work the permeability of the mushy zone is uncoupled from the predicted grain size as the characteristic length in the Kozeny Carman law is set constant. As a result, the liquid flow is not significantly affected by the inoculant distribution and only slight differences in macrosegregation formation are seen for Case 1 compared to Case 2, and the latter case is, therefore, not presented in detail. The small differences can be attributed to the difference in undercooling and its influence on macrosegregation (see Equation (3)).

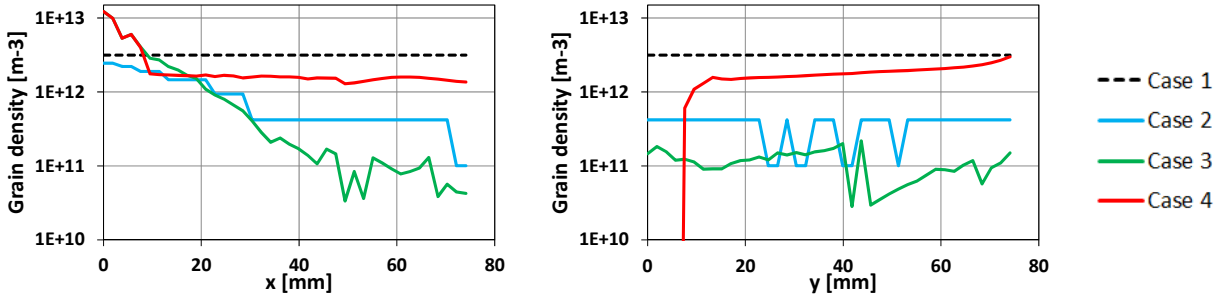

a) Horizontal profile at y=15mm b) Vertical profile at x=60mm

Figure 4. Comparison of a) horizontal and b) vertical grain density profiles for cases 1 to 4.

4.3. Case 3: Impact of inoculant motion (without grain motion)

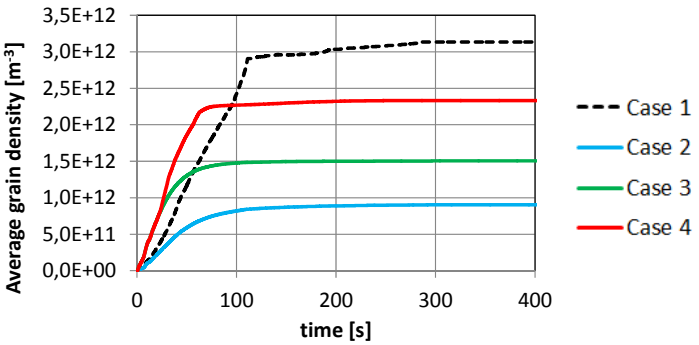

Figure 5. Evolution of the average grain density in the cavity with time.

The inoculant motion does not change the evolution of the thermal field in the cavity; therefore the differences in macrosegregation between Case 2 and Case 3are small. The microstructure, however, is strongly modified. In Figure 4a we can notice a steeper grain density gradient across the cavity, and in Figure 5we can see that globally more grains nucleate in Case 3 than in Case 2.

During the initial stages of

solidification, when the mushy zone is spreading from the chill towards the interior, the counter clockwise flow continuously brings liquid from the bulk liquid zone, carrying a high inoculant density (the inoculants in the bulk liquid were not yet activated), into the mushy zone in the top part of the cavity. If the undercooling in the mushy zone is sufficient, these additionally supplied inoculants are activated in the mushy zone. Consequently, the liquid flowing back from the mushy zone into the bulk liquid zone at the bottom of the cavity carries a low inoculant density, as can be seen in Figure 6a and c. This results in a certain inoculant segregation. On the one hand, more inoculants are supplied to the chill region, which refines its grain structure compared to Case 2, where inoculants were fixed. On the other hand, the inoculant density in the region away from the chill is diluted (Figure 6a–b), which coarsens the grain structure compared to Case 2. This explains the grain density gradient across the cavity. The inoculant segregation has however a somewhat different consequence for larger than for smaller inoculants. Large inoculants require only small undercoolings for their activation. These are easily reached across the whole cavity in Case 2 as in Case 3. The segregation of large inoculants therefore results only in a redistribution of the grain density, but does not influence the total grain population. Small inoculants require large undercoolings, which are reached only close to the chill. The segregation of small inoculants does therefore not affect the interior regions, but only increases the grain population in the chill region (Figure 6c–d). This results in an increase of the total grain population, compared to Case 2. A higher increase rate of the grain population for Case 3, seen in Figure 5 also shows that the additional grains are generated at the beginning, during the nucleation of the chill region.

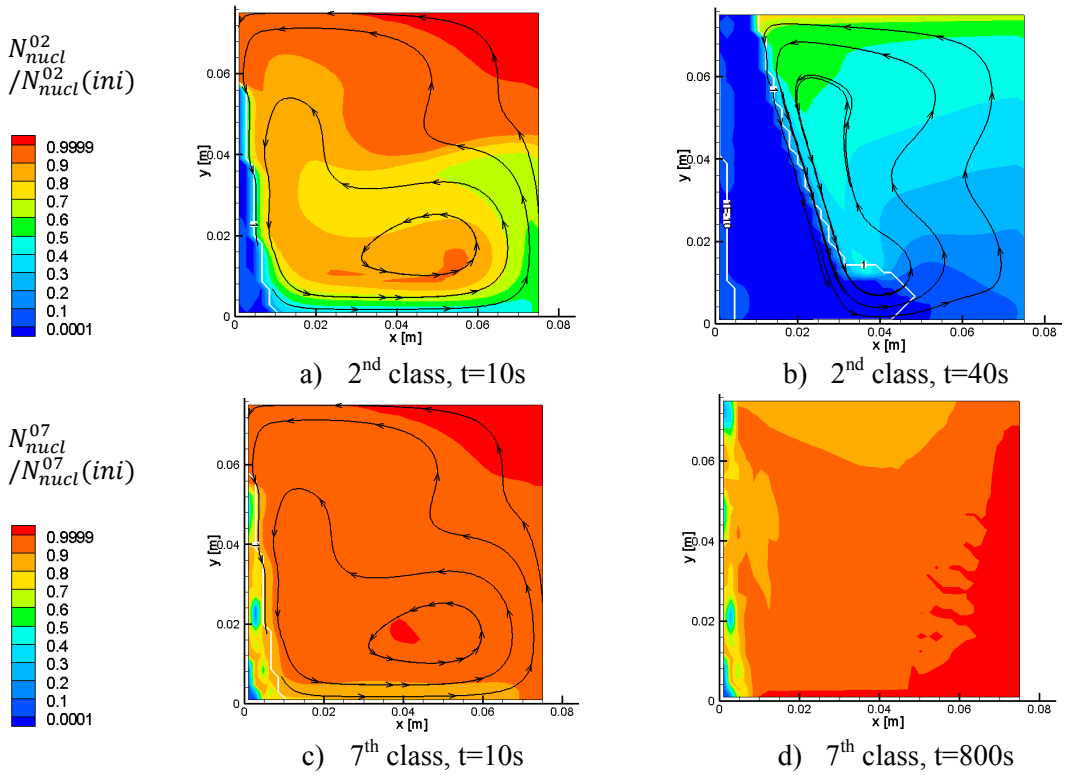

Figure 6. Maps of relative inoculant density, intrinsic liquid velocity streamlines in black and liquidus and solidus isolines in white (shown by solid fraction contour), for the 2nd and the 7th inoculant classes, at different times, for Case 3.

4.4. Case 4: Impact of grain motion

It has been seen through the first three cases that the nucleation law and the inoculant motion do not impact the macrosegregation pattern but only increase the microstructure heterogeneities. In Case 4,

the grain motion is added to these two phenomena, and differences are noticed in both microstructure and macrosegregation.

Without grain motion, the flow is counter-clockwise as the richer and colder liquid is heavier. When grain motion is added, the direction of the flow could be modified as the grains, which are lighter than the liquid, tend to float upwards along the solidification front. However, the density difference between the two phases is not high enough to do so. The average density is still increasing with the solid fraction, as can be seen in Figure, so the decrease in density due to solidification is more than compensated by the liquid enrichment and cooling. Thus the main flow direction is not modified as can be seen in Figure 7, but its pattern is totally changed as a second loop appears at the bottom. This change in flow pattern induces modifications in both macrosegregation and microstructure.

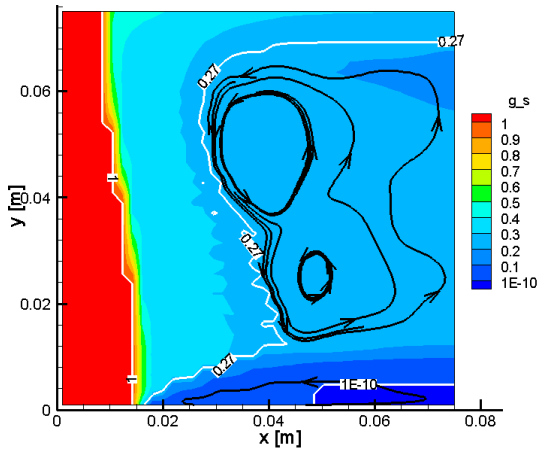

Figure 7. Map of solid fraction, liquidus, packing and solidus contours (trough solid fraction) in white and intrinsic liquid velocity streamlines in black at 120s for Case 4.

The impact of grain motion on macrosegregation can be seen by comparing the macrosegregation maps for Case 1 and Case 4 (Figure 8). The macrosegregation, which is not altered when nucleation is taken into account, is highly modified by the grain motion. The grain flotation results in accumulation of solute-lean grains towards the top of the cavity, and thus in a vertical, downward oriented concentration gradient. In Figure 7, the packing fraction isoline position is a sign of the accumulation of grains at the top. The only exception is the 10 mm thick columnar zone next to the chill, where the grains are fixed; therefore the pattern remains similar to case 3.

The microstructure is also changed by the grain motion after the columnar zone. Next to it, the newly nucleated grains are continuously swept away by the liquid. Thus the nucleation-growth competition is modified and a high undercooling is maintained. As a consequence, more grains are formed, which can be seen in Figure 5. The total number of grains increases at the same speed as in Case 3 in the columnar zone, but when the activation zone reaches the equiaxed zone, grains are formed faster. The transport of the grains leads to a more homogeneous distribution of the grain density. This is clearly seen in Figure 4a. The average grain density is higher and its distribution across the cavity is more homogeneous. The grain density also increases from the bottom to the top, as can be seen in Figure 4b, which is not surprising as the grains float.

5. Discussion and conclusion

The goal of this paper was to study the impact of the nucleation modelling and the grain motion on the microstructure and the macrosegregation formation in the case of a small casting of Al-22%Cu. We did not try to fit the experimental results, as many parameter values, as well the heat extraction rate evolution and the effective inoculant distribution are insufficiently or not at all characterized. But by studying increasingly complex modelling, tendencies are noticed and the phenomena responsible for them are identified.

The macrosegregation pattern is shown in Figure 8 for cases 1 and 4 and for the experimental data given in [7] (the values measured at the points are interpolated). We notice that the main segregation gradient is directed toward the right-bottom corner of the cavity in Case 1, and that it is almost vertical in Case 4. Qualitatively, we can compare the experimental result to these two patterns: it seems to be a combination of these two tendencies with a vertical gradient at the left side of the cavity and a gradient directed to the right-bottom corner at the end of the solidification. Thus it can be supposed that the grain motion impact is reduced at the end of solidification when only few grains remain in the mushy

zone. A more precise modelling of the grain motion, taking into account the interactions between the grains, could improve this estimation.

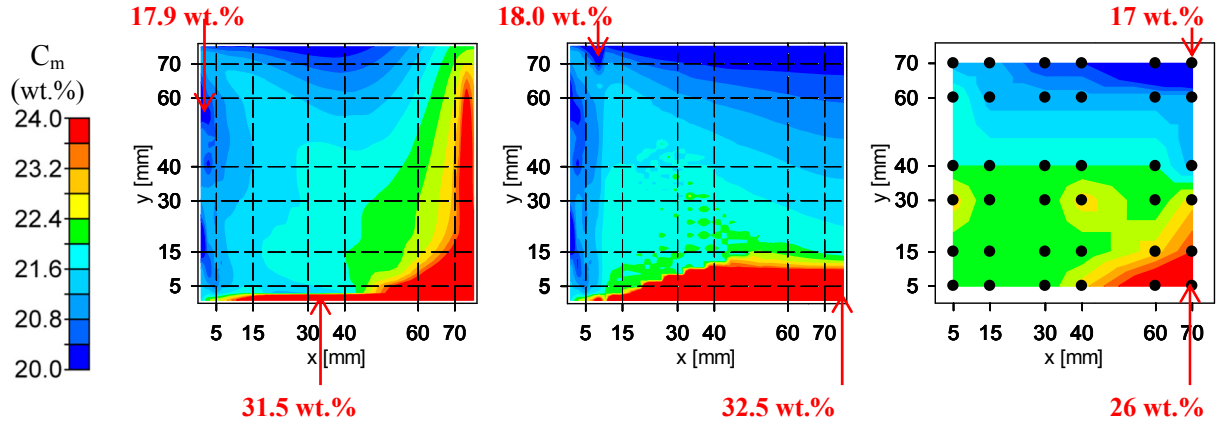

a) Case 1 b) Case 4 c) Experimental data

Figure 8. Final segregation maps for a) Case 1, b) Case 4 and c) experimental data (grid lines and points showing the measurement locations).

Inoculant motion and distribution have only small impact on the macrosegregation pattern. To check this assumption, the Case 4 was also run for a different nucleation law: inoculants were all activated at the liquidus like in Case 1. This led to the same macrosegregation pattern as for Case 4, even if the intensity of the segregation was lower.

Even though the inoculant motion has no noticeable impact on the macrosegregation, it is predominant in the microstructure formation. It is shown in this study that it increases the heterogeneities in the product (Figure 4) and that it refines the microstructure (**F**igure 5). This is the first study of the influence of inoculant on the microstructure and it shows that it seems unavoidable to take into account inoculant motion to correctly predict the microstructure.

This is a preliminary study and more work has to be done to properly estimate the inoculant distribution. Much higher undercoolings than what is usually considered in the nucleation models were found. Undercoolings of more than 5°C were calculated while in [5], the inoculant distribution is considered only up to 0.76°C. This would lead to think that finer particles than usually considered could act as nucleation sites. If it is not the case, agglomeration of inoculants or fragmentation of grains could be another explanation. In any case, this study points out the importance of the inoculants modelling, of their distribution as well as their motion, in microstructure prediction.

Acknowledgement
This research work is supported by Hydro, Alcoa Norway, Aleris, and the Research Council of Norway.

References

[1] Rappaz, M., *International Materials Reviews*, 1989. **34**(3): p. 93–124.
[2] Dantzig, J.A. and M. Rappaz, *Solidification*. 2009, Lausanne: EFPL Press.
[3] Reddy, A.V. and C. Beckermann, *Materials Processing in the Computer Age II*, 1995: p. 89-102.
[4] Stefanescu, D., et al., *Metallurgical and Materials Transactions A*, 1990. **21**(3): p. 997-1005.
[5] Greer, A.L., et al., *Acta Materialia*, 2000. **48**(11): p. 2823-2835.
[6] Zaloznik, M. and H. Combeau, *Computational Materials Science*, 2010. **48**(**1**): p. 1-10.
[7] Kumar, A., et al., *Metallurgical and Materials Transactions B*, 2011. **42**(4): **p**. 825-836.
[8] Du, Y., et al., *Materials Science and Engineering A*, 2003. **363**(1-2): p. 140-**1**51.
[9] Tronche, A., *PhD Thesis*. 2000, University of Cambridge.
[10] Tveito, K.O., et al., *IOP Conference Series: Materials Science and Engineering*, 2011(in press).